ORIGINAL ARTICLE

Journal Section

GaAsP/SiGe tandem solar cells on porous Si substrates

Pablo Caño[1]* | Manuel Hinojosa[1] | Iván García[1] | Richard Beanland[2] | David Fuertes Marrón[1] |Carmen M. Ruiz[3] | Andrew Johnson[4] | Ignacio Rey-Stolle[1]*

[1] Instituto de Energía Solar, ETSI de Telecomunicación, Universidad Politécnica de Madrid, Madrid, 28040, Spain

[2] Department of physics, University of Warwick, Coventry CV4 7AL, UK

[3] IM2NP, Aix-Marseille Université, Marseille, ~~Postal~~ 13397 ~~Code~~, France

[4] IQE plc, St. Mellons Cardiff, CF3 0LW, UK

Correspondence
Pablo Caño
Email: pablo.cano@ies-def.upm.es
Ignacio Rey-Stolle
Email: ignacio.reystolle@upm.es

Funding information
Spanish Ministerio de Cienca, Innovación y Universidades, Projects: RTI2018-094291-B-I00, ENE2017-89561-C4-2-R;
Comunidad de Madrid, Project: S2018/EMT-4308 (MADRID-PV2-CM);
Ramón y Cajal grant (RYC-2014-15621).

A GaAsP/SiGe tandem solar cell has been developed employing group IV reverse buffer layers grown on Ge/Si virtual substrates with a subsurface porous layer. Reverse buffer layers facilitate a reduction in the threading dislocation density with limited thicknesses but can induce cracks. In this new design, a porous silicon layer has been incorporated close to the Ge/Si interface. The ductility of this layer suppresses crack propagation. In terms of solar cell performance, this porous layer reduces the problem of low shunt resistance observed in previous designs and thus improves solar cell performance. The first results of this new architecture are presented here.

KEYWORDS

III-V on silicon, GaAsP/SiGe, porous silicon, reverse buffer layers, tandem on silicon.

1 | INTRODUCTION

III-V multi-junction solar cells are very efficient, breaking conversion records repeatedly in recent years [1], but still expensive for terrestrial applications. Conversely, silicon solar cells whose technology dominates the terrestrial market [2] are approaching a standstill having essentially reached their efficiency limit [3]. Therefore, the integration of III-V semiconductors on silicon substrates has been the target of

numerous research lines from the 1980s [4, 5] based on the premise of high performance III-V semiconductor multijunction solar cells combined with the low-cost advantages of large area silicon substrates [6-8]. Other alternatives for Si-based tandem solar cells have been proposed (perovskites on Si [9, 10], CdTe on Si, CIGS on Si [11], to name the most relevant), but the best device results so far have been reached with III-V/Si architectures [12].

Among the wealth of approaches to combine III-V materials and silicon for PV applications, monolithic structures are of particular interest for their straightforward integration in current manufacturing lines and lower production cost than other approaches. In this monolithic integration III-V and group-IV compounds are grown heteroepitaxially on a single substrate to produce a multijunction solar cell, which is then processed and integrated in an almost conventional way. However, the direct growth of III-V and group-IV semiconductors on silicon must tackle key difficulties such as the large differences in lattice parameter, thermal expansion coefficients or polar on non-polar growth. Therefore, smart engineering of the buffer layer between the silicon and the III-V layers is essential in order to accommodate these dissimilar parameters.

III-V/Si architectures have been demonstrated for optoelectronics with lasers [13], bipolar transistors [14], photodetectors [15] or light emitting diodes [16]. As for monolithic III-V/Si photovoltaic devices, GaAsP/Si dual junctions using GaP buffer layers [5], GaInP/GaAs tandem cells on Ge/Si virtual substrates [17] and GaAsP/SiGe dual junctions grown on inactive Si substrates have been developed [18, 19]. In the latter design an extra degree of freedom for bottom cell bandgap tunability is provided depending on the composition of the $Si_{1-x}Ge_x$ alloy. A further step ahead is the addition of minute amounts of tin to form SiGeSn alloys, which provide both bandgap and lattice constant adjustability, at the price of having to sort out big difficulties in material growth and quality [20-21]. Anyhow, $Si_{1-x}Ge_x$ alloys allow a closer approach to the optimum bandgap combination for a dual-junction solar cell [22] and have reached a significant level of maturity in terms of material growth and quality. In fact, GaAsP/SiGe tandem cells on Si have reached efficiencies over 20% [19, 23, 24]. In these structures, a $Si_{1-x}Ge_x$ buffer is grown on the silicon substrate as a graded layer, increasing Ge content until the desired Ge composition is reached [23, 25, 26]. The thickness of such buffer layers is typically between 5 and 15 μm in order to reduce the threading defect density and achieve the target bandgap (defined by the lattice parameter) while retaining sufficient quality in the surface morphology [13, 18, 23, 26]. Accordingly, this kind of graded buffer layer is known as a forward-graded buffer.

Here, an innovative architecture for the integration of III-V compounds and SiGe alloys on silicon substrates is presented, using so-called reverse-graded buffers [27, 28]. This III-V/SiGe/Si approach is aggressive in terms of growth; a germanium layer is directly grown by CVD on the silicon substrate, despite the large lattice mismatch, utilizing a growth scheme that has demonstrated dislocation densities as low as $5x10^5 cm^{-2}$. Then, a $Si_{1-x}Ge_x$ graded buffer layer is grown, decreasing from pure Ge to the desired final target (Ge ~75%). Because of the close to complete relaxation of the initial Ge layer and the reduction in lattice constant with increased silicon content, reverse-graded buffers are subject to tensile strain. The tensile strain facilitates the movement of threading dislocations, aiding their annihilation. At the same time, the increased dislocation dissociation width prevents cross-slip that is necessary for the formation of multiplication sources, eliminating dislocation pile-ups that are seen in forward-graded buffers [29] which increase threading dislocation density (TDD) and surface roughness. Reverse-graded buffers thus have both lower TDD and smoother surfaces [28, 30]. Furthermore, for Ge contents over 50%, reverse-graded buffers are thinner due to the smaller change in composition that is needed, which decreases costs [27, 31]. On the other hand, the high tensile strain gradients can result in the appearance of cracks [32] that cause a

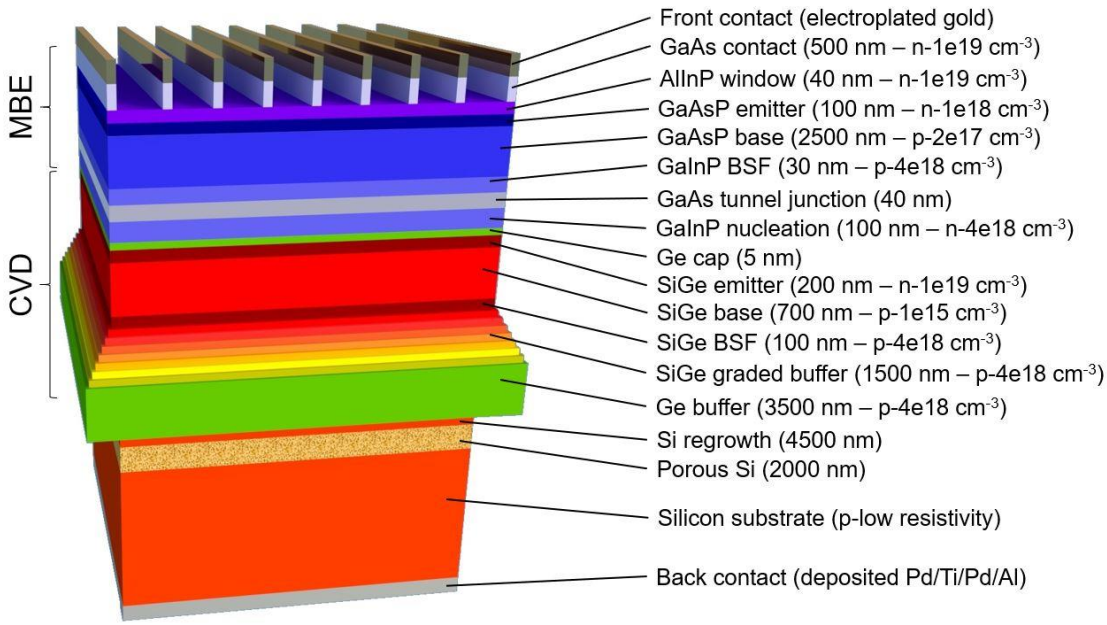

FIGURE 1. Structure of the GaAsP/SiGe tandem with porous silicon buffer layer, where the lattice constants are schematically represented. Layers with thicknesses and doping levels are labeled.

degradation in the device performance, as we have shown in previous work [33]. Therefore, in this new architecture, a porous silicon layer on the substrate subsurface has been implemented. Porous silicon has been previously used in optoelectronic [34, 35] and PV applications [36, 37] as window layers, passivation or anti-reflection coatings [38, 39]. Here, the porous silicon layer is used to absorb strain due to its higher flexibility compared to solid material [38], enhancing relaxation of the strained SiGe [40, 41, 42] and reducing the probability of fractures in the structure during thermal ramps. In addition, the cavities and pores facilitate dislocation annihilation and the nucleation of dislocation loops, which glide to the interface to form strain relieving misfit segments [43-45].

2 | EXPERIMENTAL

Fig. 1 shows the structure of the solar cells in this study with doping levels and thicknesses. The samples were grown following a combined approach using both chemical vapor deposition (CVD) and molecular beam epitaxy (MBE). Firstly, porous silicon was created by means of electrochemical etching on 6-inch (100) 6° off towards [110] silicon wafers with a resistivity of 0.01 Ωcm. Then, all group-IV layers were grown in an ASM Epsilon LPCVD reactor at a temperature of ~650 ˚C using standard precursors (SiH_4 and GeH_4 for the alloys and boron and phosphorus for the p-type and n-type doping respectively). An initial 3.5 μm germanium layer was grown directly on the silicon wafer followed by a ~1.5 mm SiGe reverse-graded buffer, changing composition gradually from pure germanium to 76% Ge. Afterwards, the $Si_{0.24}Ge_{0.76}$ bottom cell with E_g~1 eV was grown. Before the transfer to a Veeco Gen2000 MBE reactor, the $Si_{0.24}Ge_{0.76}$ bottom cell was capped with a 5 nm Ge layer in order to prevent oxidation of the Silicon in the SiGe, which is difficult to remove thermally in the MBE chamber. In the second growth III-V layers were grown lattice matched to the $Si_{0.24}Ge_{0.76}$ bottom cell, forming the tunnel junction and the $GaAs_{0.8}P_{0.2}$ top cell (E_g ~1.7 eV) [19, 47, 48] at ~650 ˚C with a growth rate of ~1 μm/h. High-resolution X-ray diffraction reciprocal space maps (RSMs) of the structures were obtained using an X'Pert Pro MRD tool.

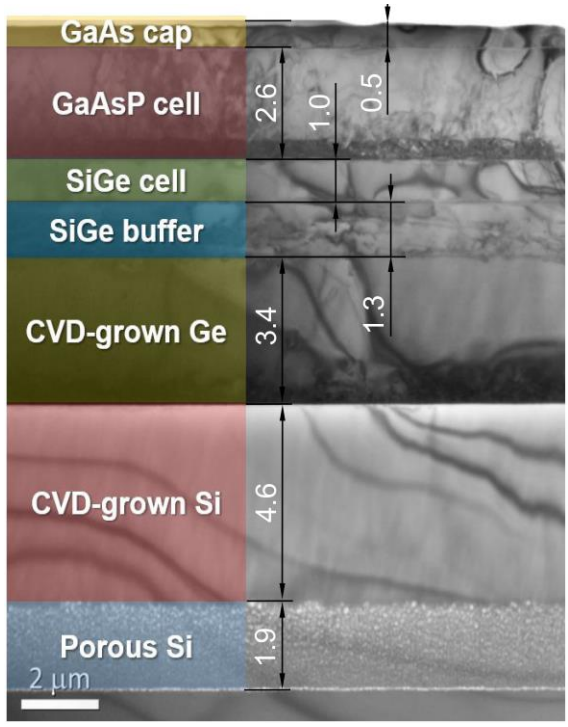

FIGURE 2. Cross-sectional bright-field transmission electron microscope image of the as-grown GaAsP/SiGe wafer, with key layers identified. The layer labeled GaAsP cell includes the tunnel junction and nucleation layer. The labels on the right indicates which layers are shown in figure 3.

An important remark about this structure should be made at this point. As shown in Fig. 1, the SiGe bottom cell is just 1 µmm thick. This value is far from the ~5-6 µmm needed for a current matched device, so our solar cells will be severely bottom cell limited. This design decision was made to minimize the risk of epilayer peel-off during the processing of the solar cells, which can be a consequence of the inclusion of porous Silicon. In our experience, the handling of large area (6 inch) wafers with thick epilayers is also not easy. Oftentimes, minor shocks during the manual handling of the wafers cause the epilayers to peel off catastrophically, ending up shattered into a thousand pieces. To minimize this risk, we limited the thickness of the bottom cell to one micron. Therefore, the goal of this study is an initial assessment the joint use of porous silicon layers and reverse graded buffers to implement functional GaAsP/SiGe tandem solar cells rather than the achievement of a high efficiency which is out of reach with a severe current mismatch.

The epi-wafers were processed into ~0.10 cm^2 (3.2 mm × 3.1 mm) solar cells with conventional photolithography techniques. Since group-IV and III-V semiconductors have different processing requirements, both front and rear contacts were specifically designed to reduce thermal budget. In this way, the high temperatures of conventional silicon metallization were avoided, minimizing the risk of crack

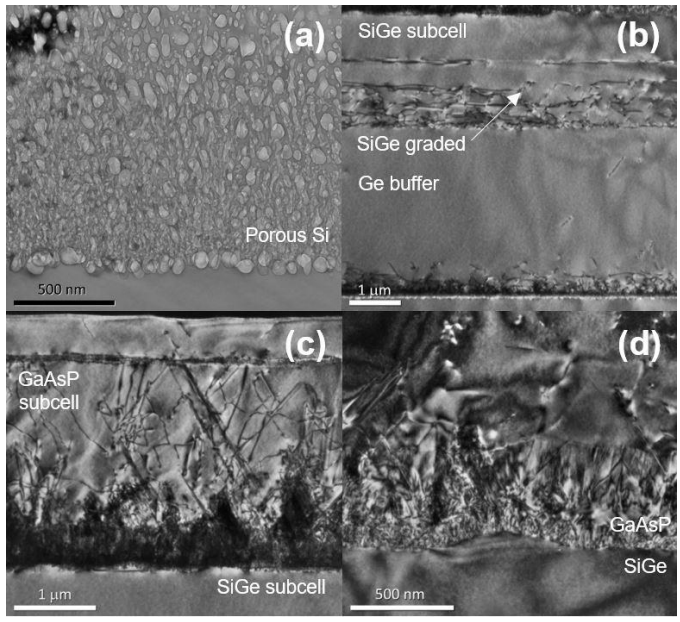

FIGURE 3. Cross-sectional TEM images of some details of the structure in Fig. 2. (a) bright-field 004 image of the porous layer; (b) dark-field 220 image of the Ge/SiGe graded buffer/ SiGe subcell; (c) dark-field 220 image of the GaAsP subcell; (d) dark-field 220 image of the GaAsP interface.

propagation and guaranteeing material compatibility. The front contact was formed using electroplated gold (~600 nm thick) without any alloying. The rear contact was deposited with Electron Beam Physical Vapor Deposition (EBPVD) and consisted of a stack of Pd(50nm) / Ti(50nm) / Pd(50nm) / Al(1000nm) alloyed at 170ºC for 600 s. No antireflection coating (ARC) was deposited on the cells.

After device fabrication, External Quantum Efficiency (EQE) was measured using a custom-made tool based on a 1000W Xe lamp, a triple-grating monochromator (JOBIN-YVON) and a lock-in amplifier. I-V curves were measured using the four-probe method with a Keithley 2602 source-meter instrument and a home-made AAA solar simulator based on a 1000-W Xe-lamp and an ORIEL 68820 stabilized power supply. Capacitance-voltage (C-V) measurements were carried out with an HP 4284 LCR meter. Curves were collected with a 5 mV signal at 30 kHz, which is considered to be high-frequency [49]. Spectral Photovoltage (SPV) measurements were performed in two-probe contact mode at room temperature using a 200W QTH-lamp filtered through a 1/8 monochromator (Oriel) as probe beam and a lock-in amplifier (Stanford).

3 | RESULTS AND DISCUSSION

3.1 | Material characterization

A cross-section of the whole structure can be observed in the Transmission Electron Microscopy (TEM) image in Fig. 2, where the most relevant layers in the structure have been identified. As can be seen, the porous silicon layer is clearly delineated between the underlying substrate and overlying CVD-grown Si. The other group-IV layers have sharp and flat interfaces with no noticeable defects. The interface between the SiGe subcell and the GaAsP top cell shows some unevenness, which is even more noticeable at the GaAsP/GaAs interface. The thicknesses of the layers agree well with the nominal values in Fig. 1. Figure 3 shows TEM images of key parts of the structure at higher magnification. Fig. 3.a shows the porous layer with a range of pore sizes, delimited by a line of large pores at the substrate interface. As discussed below, this may impact the series resistance of the cell. Fig. 3.b shows group IV layers including the Ge layer, the SiGe reverse buffer and the SiGe bottom subcell. The Ge/Si interface is very defective (as expected) but most dislocations are confined to the vicinity of the interface. In the SiGe reverse graded buffer, the interfaces between the steps are also delineated by misfit dislocations. Figure 3.c shows the GaAsP top cell and the GaAs cap layer, while Fig. 3.d shows a detail of the IV/III-V interface. In both figures the GaAsP layers appears

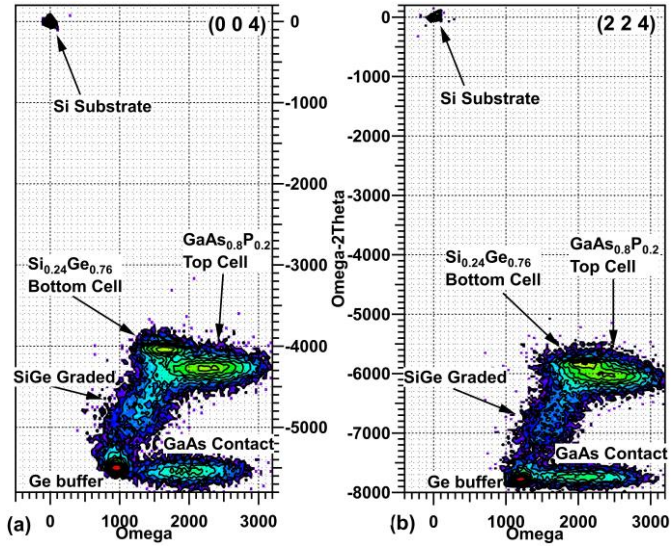

FIGURE 4. Reciprocal space maps (RSM) of the structure, including (004) reflections (a) and (224) reflections (b)

very defective, with an uneven interface with bumps and voids, and with defects –both dislocations and microtwins– propagating upwards from the defective interface.

Figure 4 shows X-ray RSMs from symmetric 004 (a) and asymmetric 224 (b) reflections of the complete structure. The different layers in the structure can be identified and their lattice mismatch and composition quantified. The silicon substrate peak is clearly visible in the upper left part of the graph. The Ge buffer peak can be observed with a mismatch of 4.36%, as deduced from the maps. Then, the diffracted intensity from the SiGe graded buffer layer spreads from the Ge peak to the SiGe bottom cell peak, with a composition of $Si_{0.24}Ge_{0.76}$. The $GaAs_{0.8}P_{0.2}$ layers grown on top are found to be slightly lattice-mismatched under compressive strain, which could be contributing to the poor quality of these layers. In fact, these III-V semiconductor layers (GaAs contact and GaAsP top cell) show a lower crystallographic quality, as indicated by their high peak FWHM, consistent with was observed in Figs. 3.c and 3.d. The threading dislocation density (TDD) of the full structure could not be measured. However, the cross section TEM images shown (Fig. 3.c) indicate a high value (~10^9 cm^{-2}). Concerning the SiGe bottom cell, in a previous work where similar structures were grown on standard silicon wafers, a TDD of ~$8x10^5$ cm^{-2} was measured [33]. This level is comparable to TDDs reported in other studies of forward buffers in $Si_{1-x}Ge_x$ with x ~80% [50-52] and thus suggests that the challenge of these structures relies more on the optimization the epitaxial growth conditions for porous silicon substrates rather than the use of reverse graded buffers.

On the wafer surface, some cracks are still visible to the naked eye, although the crack density has been significantly reduced as compared with growths on standard Si substrates with equally thin bottom subcells [33].

3.2 Solar Cell results

Fig 5.a shows in red the experimental External Quantum Efficiency (EQE) of the top cell in the GaAsP/SiGe solar cells grown on porous Si substrates. The EQE of a solar cell with the same structure –*i.e.* also with a thin 1 mm SiGe bottom cell– but manufactured on standard Si wafers is included for reference in blue. The response of the new design has clearly improved and the bandgap obtained from a linear fit of the final tail of the EQE (E_g~1.64 eV) agrees well with the $GaAs_{0.8}P_{0.2}$ composition determined from the reciprocal space maps, which according to Vegard's law should correspond to an E_g = 1.67 eV. However, the EQE reaches a maximum of ~50% whereas other works in the literature for similar devices grown by MBE report clearly higher EQEs, as can be observed in the green line corresponding to GaAsP solar cell grown by Grasmann and coworkers on Si with GaP nucleation layers and GaAsP graded buffers [53]. We choose to benchmark our

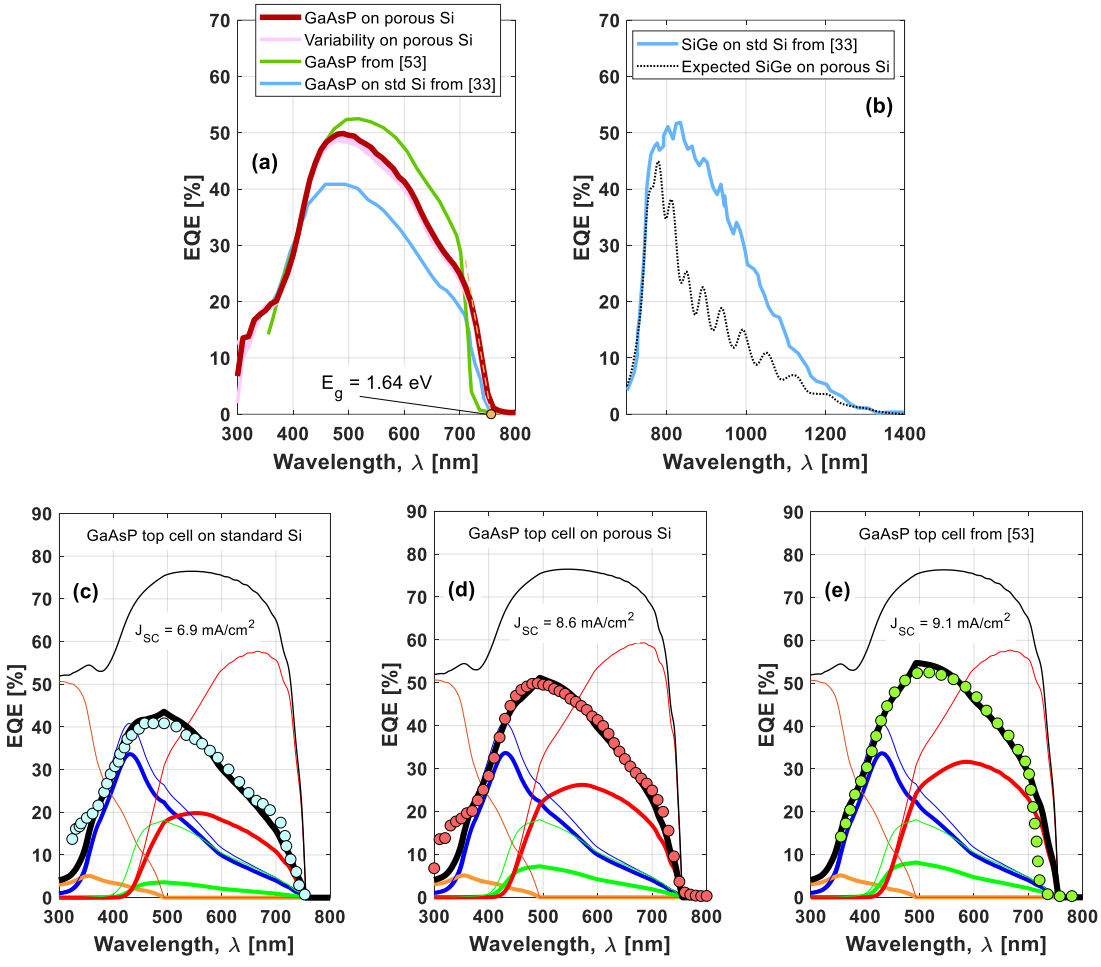

FIGURE 5. Experimental and simulated EQEs of the GaAsP/SiGe tandem solar cells on porous silicon in comparison with other results from the literature. (a) Experimental EQE of the best GaAsP cell grown on porous silicon (thick red line); thin pink lines represent the EQE of other devices in the same wafer to give an idea of performance homogeneity; a linear fit to obtain the bandgap has been included as a dashed line; EQE of the best GaAsP top cell grown on standard silicon wafers (blue line) [33]; EQE of a GaAsP top cell taken from [53] as a benchmark (green line). (b) Experimental EQE of the SiGe subcell grown on standard silicon wafers (blue line) [33]; expected EQE of SiGe bottom cell grown on porous Si substrates. (c) Simulation of the EQE of the GaAsP to cells in GaAsP/SiGe tandems grown on standard Si substrates, (taken from [33]). (d) Simulation of the EQE of the GaAsP to cells in GaAsP/SiGe tandems grown on porous Si substrates (this work); (e) Simulation of the EQE of the GaAsP to cells in GaAsP/Si tandems (taken from [53]). Round symbols correspond to the experimental data. The thick black line is the total simulated EQE whereas the thin black line corresponds to total absorptance. The thick colored lines correspond to the contributions of each layer: orange for the window, blue for the emitter, green for the space charge region and red for the base. The thin colored lines are the absorptance in each layer with the same color code. The J_{sc} obtained from the integration of the experimental EQE over the AM1.5G spectrum is included in each graph.

results with [53] since the GaAsP top cell has a similar structure – though with a slightly higher bandgap – was also grown by MBE and also underwent a reactor transfer prior to the growth of the top cell. There are

better results in the literature [48, 54, 55] that we do not use as a benchmark simply because they were either grown with notably different structures or techniques (MOVPE), or lack sufficient structural information.

Fig. 5.b shows in a black dashed line the expected (*i.e.* simulated) EQE from the SiGe bottom cell that could not be actually measured. In our previous work, the EQE of 1 mm thick SiGe bottom subcells could not be measured either. However, as shown in a blue line in Fig. 5.b, the EQE of thicker SiGe subcell designs (5 mm) could be measured and thus a functional GaAsP/SiGe tandem solar cell on silicon was demonstrated [33]. However, in the structure grown on porous Silicon only the top cell EQE could be measured, even though several samples were grown and many solar cells were manufactured and tested. The lack of bottom cell response will be discussed later.

In order to gain some insight into the performance differences of the top cells, EQE simulations were made using an analytic model [56]. Figures 5.c to 5.e present the results of these simulations for GaAsP subcells grown on: standard Si (Fig. 5.c) [33]; porous Si (Fig. 5.d) (this work); and our reference device from the literature (Fig. 5.e) [53]. In figures 5.c to 5.e, circles correspond to the experimental data of Fig. 5.a and lines account for the modelling. The thick black line in each panel is the calculated total EQE whereas each thin black line corresponds to the total absorptance in the top cell (i.e. the ideal EQE with unity collection efficiency). Thick colored lines correspond to the contributions of each layer with the color code as indicated in the figure caption, whereas their thin counterparts again correspond to the absorptance in each layer. Therefore, the difference between thick and thin lines of the same color gives a visual indication about how close (or far) a layer is from perfect collection efficiency. Comparing the calculated EQE with the absorptance, it can be concluded that the response of all GaAsP top cells clearly shows room for significant improvement. In the case of the emitter (blue lines), very similar responses are found in the three designs. In all cases it could be fitted with a diffusion length of ~100 nm, which coincides with the emitter thickness in the three cases. In fact, this yields a reasonable blue response of the three devices. However, the base and space charge region are clearly different in the three designs. The response of the base is some way below the corresponding absorptance curve (thin red lines). In addition, the three designs behave quite differently: we see a remarkably low response in the cells grown on standard Si (Fig. 5.c), which could be fitted with a diffusion length of ~200 nm; there is a very low response in the cells grown on porous Si (Fig. 5.d), which could be fitted with a diffusion length of ~350 nm; and we find a low response in the cells from [53] (Fig. 5.e), which could be fitted with a diffusion length of ~550 nm. In all three cases, the diffusion lengths are notably smaller than the base layer thickness (2 mm) and thus the collection efficiency is deleteriously

affected. Regarding the space charge region, some differences in collection efficiency are observable too. In each case, it was necessary to simulate the space charge region (SCR) with a collection probability similar to that of the quasi-neutral base in order to obtain a reasonable fit of the experimental curve. If unity collection efficiency was assumed for the SCR (as in Hovel's equations [56]), no fit was possible.

Since the three GaAsP top cell structures are very similar, these simulation results can be understood as progress towards a better crystallographic quality in each design, though still reaching far from perfect minority carrier collection in the SCR and base. Other than the evident effect of TDD, it has been reported that the GaAsP epitaxial growth conditions influence material quality in a poorly understood way [54]. We therefore believe that there is an ample margin for improvement of these results by tuning the growth conditions, considering that this is our first attempt to grow tandem cells on porous Si substrates.

Coming back to the lack of response in the SiGe bottom cell, it should be noted that the situation here resembles that of a GaInP/Ga(In)As/Ge triple junction solar cell (3JSC) where the EQE of the germanium bottom cell is frequently unmeasurable for a number of reasons [57, 58]. The emitter of our SiGe cell is formed during the growth of the GaInP nucleation layer –as in Ge subcells in 3JSCs– by the concurrent in-diffusion of P, but also of Ga and In, and out-diffusion of Ge from the capping layer. Such a strong atom exchange at the III-V/IV heterointerface, in a material with a high TDD, may produce a p-n junction exhibiting both a low shunt resistance and a low breakdown voltage, which are typical causes for an unmeasurable bottom cell [59].

I-V curves under one-sun illumination (AM1.5d ASTM G173 spectrum) of the GaAsP/SiGe tandem cells are presented in Fig. 6a for the design on porous silicon (red and pink curves) and standard silicon wafers (blue). Again, the red line represents the best device, whilst the thin pink lines are the I-V curves of other cells in the same wafer and thus give an idea of device-to-device variability. The short-circuit current density (J_{SC}= 8.9 mA/cm^2) is in agreement with the measured EQE, and is obviously low, which is a result of the collection problems discussed around the EQE curves, remembering that the cells have no ARC. Looking at the shape of the curve around V_{OC}, the impact of a parasitic diode in reverse bias is also evident, though it has been greatly alleviated in the new structure, which we address below. Apart from this parasitic diode the most remarkable features in the I-V curves are the limited FF and low V_{OC} in both designs. In the case of tandem cells grown on conventional Si substrates, the low shunt resistance is very evident in the I-V curve, causing deleterious effects in both FF and V_{OC}. In [33] it was argued that the low R_{shunt} was caused by a high

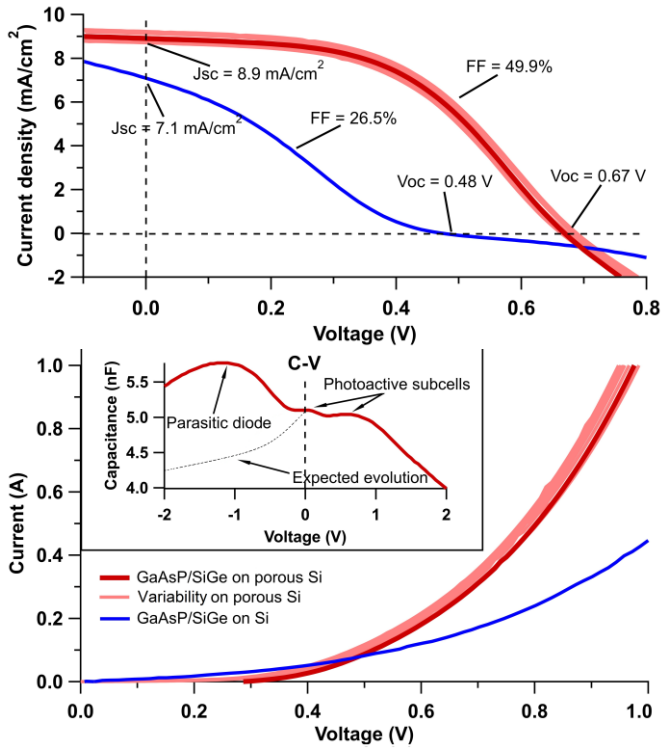

FIGURE 6. (Top panel) Lighted I-V curve of the best GaAsP/SiGe tandem cell grown on porous silicon (thick red line); the thin pink lines represent the I-V curves of most of the devices measured and give an idea of the device-to-device variability; as reference, the illuminated I-V curve of the best GaAsP/SiGe tandem cell grown on standard silicon substrates has been included (blue line) [33]. (Bottom panel) Dark I-V curves of the solar cells following the same color coding. Inset: C-V curve of a representative device obtained at 300 K under dark conditions. Labels indicate the signature of the different p-n junctions. The thin dashed line qualitatively shows the expected trend without a parasitic diode.

crack density in the cell, which behave both as efficient recombination centers for minority carriers and as electrical shorts. However, in the samples grown on porous Si substrates, clear improvements in both FF (from 26.5% to 48.6%) and V_{oc} are observed (from 0.48 to 0.67 V), as a result of much lower crack densities. Values are still low but the improvement is evident. In Fig. 6 (bottom) the dark I-V curves of the GaAsP/SiGe tandems are plotted following the same color code as in Fig. 6 (top). The shunt resistances can be visually compared between both structures, being much higher in the porous silicon design.

Porous silicon has been reported to have a low electrical conductivity [34-37], so its impact on series resistance is a possible concern. However, the presence of the parasitic junction complicates the assessment of the series resistance from the J-Vs in Fig. 6.

In order to confirm the presence of a parasitic diode, C-V measurements were performed on the samples (Fig. 6, bottom inset). The detailed understanding of C-V curves in multijunction solar cells is not straightforward, since only the voltage across the device terminals is known and no information is available about the particular bias at each subcell [60-62]. However, in this case we simply intend to detect the signature of a parasitic diode in reverse bias. The inverse of the total capacitance of the multijunction solar cell (C_T) equals the sum of the inverse of the capacitance of each junction in the device (C_i):

$$\frac{1}{C_T} = \sum_i \frac{1}{C_i} \qquad (1)$$

In principle, in well-behaved cells, it is reasonable to assume that neither the metal/semiconductor contacts nor the tunnel junctions contribute to C_T. In particular, tunnel junctions, being nominally ultra-highly doped, should have a very high junction capacitance and therefore should play a negligible effect in the sum of inverses, which is dominated by the smallest contributions [60]. So in Eq. (1) only capacitance contributions from p/n junctions should be present. As reported by Ruiz et al. in [60], the C-V curve of a dual junction solar cell with a good tunnel junction would show two humps in the first quadrant –one for each subcell–, a roll-

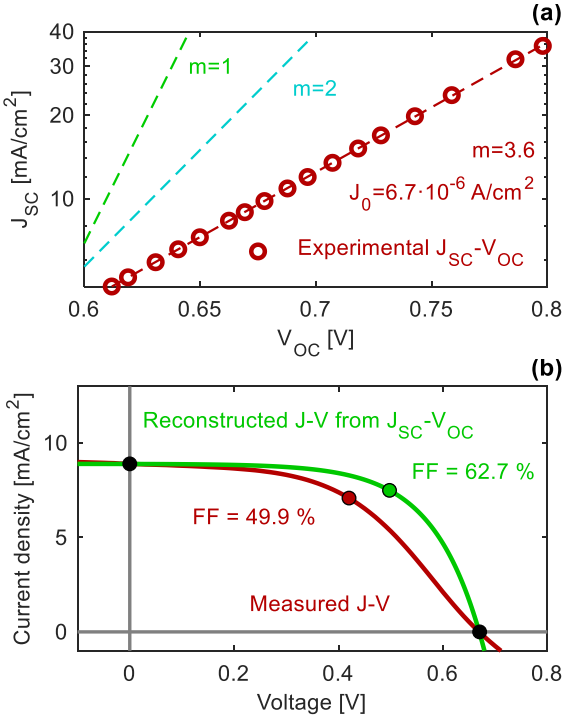

FIGURE 7. (a) J_{SC}–V_{OC} curve of a GaAsP/SiGe tandem cell grown on a porous Si substrate and subsequent fit. (b) Reconstructed illuminated J-V from the J_{SC}-V_{OC} data and measured lighted curve.

off at high positive voltages, whereas at low positive voltages and under reverse bias the capacitance should steadily decline to its lowest value. We performed C-V measurements at 300K under dark conditions and obtained the curve in the inset of Fig. 6 (bottom). In the positive voltage range, we find the two humps expected followed by the fall of capacitance at high voltages (V>1.3V). These two peaks correspond to the GaAsP and SiGe junctions and, in the second quadrant, we would expect to observe a decline in the capacitance associated with the extension of their space charge regions at negative bias [60]. Instead, we find a third peak that we interpret as a third junction in reverse polarity since it shows the expected behavior for the first quadrant but in the second, namely, a fall in capacitance at high voltages, then a peak and finally a decline as we approach 0 volts. This is the signature of a p/n junction in reverse bias, namely, a parasitic junction, as anticipated from the lighted I-V curves in Fig. 6 (top). We hypothesize that this diode is probably related to the tunnel junction or an adjacent layer. In conventional multijunction cells on Ge substrates, it has been reported that Ge can diffuse over 300 nm into the GaInP nucleation layer, producing strong n-type background doping [63]. In our structure, we have an analogous situation in which a 100 nm n-type GaInP nucleation layer is grown on a Ge cap layer (see Fig. 1). It is possible that Ge diffusion during the growth of the GaAsP top cell may reach the tunnel junction p-side –or its cladding layer– reversing its polarity or partially compensating its nominally high doping. This would produce a diode in reverse polarity. The growth of a thicker GaInP nucleation layer could avoid this issue in the future.

In order to get rid of the influence of the parasitic diode and assess the performance limits of the device, we measured the I-V curve at different irradiances and performed a J_{SC}-V_{OC} analysis as shown in Fig 7.a. The J_{SC}-V_{OC} line follows a clear logarithmic trend corresponding to an ideality factor of n=3.6 and a reverse saturation current density of $J_0 = 8.5 \cdot 10^{-3}$ A/cm^2. An ideality factor of 3.6 is in agreement with a device being limited by recombination either in the space charge region or at the junction perimeter, or most likely a combination of both. A high perimeter recombination may be linked to exposed facets in cracks. A high recombination rate within the space charge region is also consistent with the abundance of defects and with the simulations of the EQE, where limited collection in this region had to be assumed. The reconstructed I-V from J_{SC}-V_{OC} measurements is shown in Fig. 7.b together with the experimental I-V. The FF of the reconstructed curve is 63.2%, much better than the real I-V, though still far from the ~80% reported for GaAsP top cells in the best results from the literature [53, 54]. This indicates that, even leaving aside resistive and parasitic diode effects, recombination losses still impact severely the performance of the solar cells. This is another argument for improvement in the crystallographic quality of the GaAsP top cell as an imperative. In this

regard, the GaAsP material quality may be compromised due to the fact that it was grown by MBE. There is a lot of evidence that III-V nucleation on Ge –note that the III-V growth takes place on the thin Ge cap (see Fig. 1)– is much more challenging when using MBE vs MOVPE [53], [64]. We are confident that improvements in GaAsP material quality and top cell performance will be demonstrated using III-V material grown by MOVPE.

The above J_{SC}-V_{OC} analysis is not a direct proof of a working bottom cell. To verify the existence of a working SiGe bottom cell, spectral photovoltage (SPV) measurements were made. The advantage of SPV over EQE is its higher signal to noise ratio and its immunity to series resistance effects. Fig. 8.a shows the SPV response of the GaAsP top cell (in yellow) and SiGe bottom cell (in red). The upsurge in the signal occurs at the bandgap energy in each case (i.e. the energy above which the device is capable of generating voltage), whereas the drop-off is associated with the low-pass filter used in each case. The smoother photovoltage increase observed in the bottom subcell is in agreement with the indirect nature of the SiGe bandgap. On the other hand, the GaAsP top cell shows a sharper edge, related to the expected direct bandgap associated with the P-content, about 20% in this alloy. Fig. 8.b and 8.c depict the fits to obtain the bandgap energies for the GaAsP top cell and SiGe bottom cell, respectively. In the case of the GaAsP, as a direct bandgap material, the

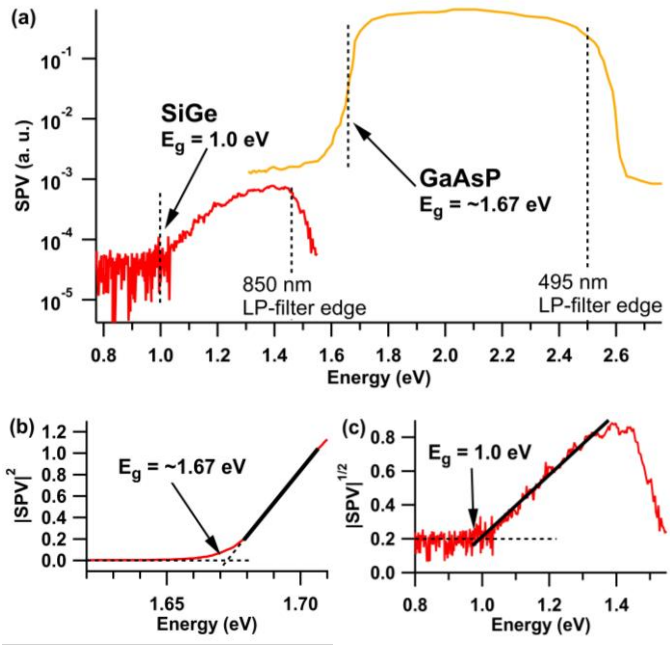

FIGURE 8. (a) Spectral photovoltage measurements of the GaAsP/SiGe tandem cells grown on porous substrates. The red curve corresponds to the bottom cell responses whereas the yellow curve is that of the GaAsP top cell. (b) Fit for obtaining the GaAsP top cell bandgap energy. (c) Fit for obtaining the SiGe bottom cell bandgap energy.

SPV signal squared at energies close to the bandgap has been assumed to be proportional to the bandgap energy. In the case of the SiGe, as an indirect bandgap material, it is the square root of SPV, which is proportional to E_g for energies near the bandgap energy. The values obtained from the fits agree well with the target design values as well as with the fit obtained from the EQE of the top cell. As a concluding point for this study, these responses in the SPV signal demonstrate the existence of a tandem GaAsP/SiGe solar cell.

Conclusions

We demonstrate a new pathway for III-V compound integration on silicon for photovoltaic applications. A GaAsP/SiGe tandem solar cell has been grown on porous silicon substrates through group IV reverse graded buffer layers. Although they can reduce the threading dislocation density and allow the growth of thinner buffers, reverse buffers have shown to be prone to cracking. This new design uses a porous silicon layer incorporated in the substrate to increase its flexibility. In comparison with similar solar cell structures grown on standard substrates, the porous silicon has (i) decreased the number of visible cracks, (ii) increased shunt resistance, (iii) improved top cell spectral response and (iv) improved the V_{OC} and FF of the cells, though the overall performance of this particular device still remains below similar architectures grown on forward graded buffers or on GaP/Si templates. In spite of the issues observed and analyzed, the existence of a tandem GaAsP/SiGe solar cell has been demonstrated and a clear improvement over analogous designs grown on standard silicon wafers has been attained. We are confident that improvements in GaAsP material quality and top cell performance will be demonstrated using III-V material grown by MOVPE.

ACKNOWLEDGEMENTS

The technical assistance of Mr. Luis Cifuentes and Mr. Jesús Bautista for solar cell manufacturing and characterization are greatly appreciated.

REFERENCES

[1] M. A. Green, Y. Hishikawa, E. D. Dunlop, D. H. Levi, J. Hohl-Ebinger, A. W. Y. Ho-Baillie, "Solar cell efficiency tables (version 51),"Progress in Photovoltaics: Research and Application s, vol. 26, (1), pp. 3-12, 2018.

[2] C. Battaglia, A. Cuevas,S. De Wolf, "High-efficiency crystalline silicon solar cells: status and perspectives,"Energy & Environmental Science, vol. 9, (5), pp. 1552-1576, 2016.

[3] K. Yoshikawa et. al., "Exceeding conversion efficiency of 26% by heterojunction interdigitated back contact solar cell with thin film Si technology,"Solar Energy Materials and Solar Cells, vol. 173, pp. 37-42, 2017.

[4] T. Suzuki, T. Soga, T. Jimbo, M. Umeno, "Growth mechanism of GaP on Si substrate by MOVPE,"Journal of Crystal Growth, vol. 115, (1-4), pp. 158-163, 1991.

[5] K. Hayashi, T. Soga, H. Nishikawa and T. Jimbo, "MOCVD growth of GaAsP on si for tandem solar cell application," in IEEE Photovoltaic Specialists Conference, Hawaii, USA, 1994, .

[6] K. Hayashi, T. Soga, H. Nishikawa, T. Jimbo and M. Umeno, "MOCVD growth of GaAsP on si for tandem solar cell application," in Conference Record of the IEEE Photovoltaic Specialists Conference, 1994, pp. 1890-1893.

[7] S. Kurtz, D. Myers, W. E. McMahon, J. Geisz,M. Steiner, "A comparison of theoretical efficiencies of multi-junction concentrator solar cells,"Progress in Photovoltaics: Research and Applications, vol. 16, (6), pp. 537-546, 2008.

[8] O. Supplie et. al., "Metalorganic vapor phase epitaxy of III–V-on-silicon: Experiment and theory,"Progress in Crystal Growth and Characterization of Materials, vol. 64, (4), pp. 103-132, 2018.

[9] S. Essig et. al., "Raising the one-sun conversion efficiency of III–V/Si solar cells to 32.8% for two junctions and 35.9% for three junctions,"Nature Energy, vol. 2, (9), pp. 17144, 2017.

[10] T. Leijtens, K. A. Bush, R. Prasanna,M. D. McGehee, "Opportunities and challenges for tandem solar cells using metal halide perovskite semiconductors,"Nature Energy, vol. 3, (10), pp. 828-838, 2018.

[11] J. Ramanujam,U. P. Singh, "Copper indium gallium selenide based solar cells – a review,"Energy & Environmental Science, vol. 10, (6), pp. 1306-1319, 2017.

[12] M. Feifel, D. Lackner, J. Ohlmann, J. Benick, M. Hermle, D. Dimroth, "Direct Growth of a GaInP/GaAs/Si Triple-Junction Solar Cell with 22.3% AM1.5g Efficiency,"RRL Solar, vol. 3, (12), 2019.

[13] M. E. Groenert et. al., "Monolithic integration of room-temperature cw GaAs/AlGaAs lasers on Si substrates via relaxed graded GeSi buffer layers,"Journal of Applied Physics, vol. 93, (1), pp. 362-367, 2003.

[14] K. L. Lew et. al., "High gain AlGaAsGaAs heterojunction bipolar transistor fabricated on SiGeSi substrate,"Journal of Vacuum Science and Technology B: Microelectronics and Nanometer Structures, vol. 25, (3), pp. 902-905, 2007.

[15] H. Luan et. al., "High-quality Ge epilayers on Si with low threading-dislocation densities,"Applied Physics Letters, vol. 75, (19), pp. 2909-2911, 1999.

[16] V. K. Yang et. al., "Monolithic integration of III-V optical interconnects on Si using SiGe virtual substrates,"Journal of Materials Science: Materials in Electronics, vol. 13, (7), pp. 377-380, 2002.

[17] R. Ginige et. al., "Characterization of Ge-on-Si virtual substrates and single junction GaAs solar cells,"Semiconductor Science and Technology, vol. 21, (6), pp. 775-780, 2006.

[18] K. J. Schmieder, A. Gerger, M. Diaz, Z. Pulwin, C. Ebert, A. Lochtefeld, R. Opila, A. Barnett, "Analysis of Tandem III-V/SiGe Devices Grown on Si,"PV Specialist Conference, 38th IEEE, 2012.

[19] A. J. Pitera, J. Hennessy, A. C. Malonis, E. A. Fitzgerald and S. A. Ringel, "Monolithically integrated thin film III-V/Si solar panel on wafer for active power management," in Conference Record of the IEEE Photovoltaic Specialists Conference, 2011, pp. 003703-003706.

[20] R. Roucka et. al., "Demonstrating Dilute-Tin Alloy SiGeSn for Use in Multijunction Photovoltaics: Single- and Multijunction Solar Cells With a 1.0-eV SiGeSn Junction,"IEEE Journal of Photovoltaics, vol. 6, (4), pp. 1025-1030, 2016.

[21] R. A. Soref,C. H. Perry, "Predicted band gap of the new semiconductor SiGeSn,"Journal of Applied Physics, vol. 69, (1), pp. 539-541, 1991.

[22] J. P. Connolly, D. Mencaraglia, C. Renard, D. Bouchier, "Designing III-V multijunction solar cells on silicon,"Progress in Photovoltaics: Research and Applications, vol. 22, (7), pp. 810-820, 2014.

[23] L. Wang et. al., "Current matched three-terminal dual junction GaAsP/SiGe tandem solar cell on Si,"Solar Energy Materials and Solar Cells, vol. 146, pp. 80-86, 2016.

[24] B. Conrad et. al., "Improved GaAsP/SiGe tandem on silicon outdoors and under concentration," in 2017 IEEE 44th Photovoltaic Specialist Conference, PVSC 2017, 2018, pp. 1-5.

[25] E. A. Fitzgerald et. al., "Relaxed GexSi1-x structures for III-V integration with Si and high mobility two-dimensional electron gases in Si,"vol. J. Vac. Sci. Technol. B 10(4), 1992.

[26] J. Faucher et. al., "Single-junction GaAsP solar cells grown on SiGe graded buffers on Si,"Applied Physics Letters, vol. 103, (19), 2013.

[27] V. A. Shah, A. Dobbie, M. Myronov, D. J. F. Fulgoni, L. J. Nash, D. R. Leadley, "Reverse graded relaxed buffers for high Ge content SiGe virtual substrates,"Applied Physics Letters, vol. 93, (19), 2008.

[28] G. Capellini et. al., "Strain relaxation in high Ge content SiGe layers deposited on Si,"Journal of Applied Physics, vol. 107, (6), pp. 063504, 2010.

[29] G. P. Watson, E. A. Fitzgerald, Y. H. Xie, D. Monroe, "Relaxed, low threading defect density Si0.7Ge0.3 epitaxial layers grown on Si by rapid thermal chemical vapor deposition," Journal of Applied Physics, vol. 75(1), pp. 263-269, 1994.

[30] T. Ward, A. M. Sanchez, M. Tang, J. Wu, H. Liu, D. J. Dunstan, R. Beanland, "Design rules for dislocation filters,"Journal of Applied Physics, vol. 116, 2014.

[31] Y. H. Xie et. al., "Semiconductor Surface Roughness: Dependence on Sign and Magnitude of Bulk Strain,"Physical Review Letters, vol. 73, (22), pp. 3006-3009, 1994.

[32] V. A. Shah, A. Dobbie, M. Myronov, D. R. Leadley, "Reverse graded SiGe/Ge/Si buffers for high-composition virtual substrates,"Journal of Applied Physics, vol. 107, (6), 2010.

[33] P. Caño et. al., "Hybrid III-V/SiGe solar cells grown on Si substrates through reverse graded buffers,"Solar Energy Materials and Solar Cells, vol. 205, pp. 110246, 2020.

[34] J. P. Zheng, K. L. Jiao, P. Shen, W. A. Anderson, H. S. Kwok, "Highly sensitive photodetector using porous silicon,"Applied Physics Letters, vol. 61, pp. 459, 1998.

[35] C. Tsai, K. H. Li, J. C. Campbell, "Rapid-thermal-oxidised porous Si photodetectors,"Electronics Letters, vol. 29, (1), pp. 134, 1993.

[36] G. Smestad, M. Kunst,C. Vial, "Photovoltaic response in electrochemically prepared photoluminescent porous silicon,"Solar Energy Materials and Solar Cells, vol. 26, (4), pp. 277-283, 1992.

[37] P. E. Jiménez-Cruz, A. Dutt, B. de la Mora, G. Santana, "Porous silicon infiltration with advanced materials for their use in third generation of solar cells,"IEEE 7th World Conference on Photovoltaic Energy Conversion, 2018.

[38] P. Menna, G. Di Francia,V. La Ferrara, "Porous silicon in solar cells: A review and a description of its application as an AR coating,"Solar Energy Materials and Solar Cells, vol. 37, (1), pp. 13-24, 1995.

[39] A. Prasad, S. Balakrishnan, S. K. Jain, G. C. Jain, "Porous silicon oxide anti-reflection coating for solar cells,"Journal of the Electrochemical Society, vol. 129(3), 1982.

[40] S. Hasegawa, K. Maehashi, H. Nakashima, T. Ito,A. Hiraki, "Growth and characterization of GaAs films on porous Si,"Journal of Crystal Growth, vol. 95, (1), pp. 113-116, 1989.

[41] K. Barla, R. Herino, G. Bomchil, J. C. Pfister,A. Freund, "Determination of lattice parameter and elastic properties of porous silicon by X-ray diffraction,"Journal of Crystal Growth, vol. 68, (3), pp. 727-732, 1984.

[42] D. M. Follstaedt, S. M. Myers, J. A. Floro,S. R. Lee, "Interaction of cavities with misfit dislocations in SiGe/Si heterostructures,"Nuclear Instruments and Methods in Physics Research Section B: Beam Interactions with Materials and Atoms, vol. 127-128, pp. 375-378, 1997.

[43] B. Holländer et. al., "Enhanced strain relaxation of epitaxial SiGe layers on Si(100) after H+ ion implantation,"Nuclear Instruments and Methods in Physics Research Section B Beam Interactions with Materials and Atoms, vol. 148(1), pp. 200-205, 1999.

[44] H. Trinkhaus et. al., "Strain relaxation mechanism for hydrogen-implanted Si1-x Gex/Si(100) heterostructures,"Applied Physics Letters, vol. 76(24), pp. 3552, 2000.

[45] M. Raïssi, G. Regula,J. Lazzari, "Low-defect metamorphic Si (Ge) epilayers on Si (001) with a buried template of nanocavities for multiple-junction solar cells,"Solar Energy Materials and Solar Cells, vol. 144, pp. 775-780, 2016.

[46] L. Wang et. al., "Current matched GaAsP/SiGe tandem device on si over 20% efficiency under indoor measurement," in 2015 IEEE 42nd Photovoltaic Specialist Conference, PVSC 2015, 2015.

[47] M. Diaz et. al., "Tandem GaAsP/SiGe on Si solar cells,"Solar Energy Materials and Solar Cells, vol. 143, pp. 113-119, 2015.

[48] P. Caño et. al., "Hybrid III-V/SiGe solar cells on si substrates and porous si substrates," in IEEE 46th Photovoltaic Specialists Conference (PVSC), Chicago, 2019 IEEE 46th Photovoltaic Specialists Conference (PVSC), pp. 2513-2518.

[49] F. Recart,A. Cuevas, "Application of junction capacitance measurements to the characterization of solar cells,"IEEE Transactions on Electron Devices, vol. 53, (3), pp. 442-448, 2006.

[50] S. A. Ringel et. al., "Single-junction InGaP/GaAs solar cells grown on Si substrates with SiGe buffer layers,"Progress in Photovoltaics: Research and Applications, vol. 10, (6), pp. 417-426, 2002.

[51] M. E. Groenert et. al., "Monolithic integration of room-temperature cw GaAs/AlGaAs lasers on Si substrates via relaxed graded GeSi buffer layers,"Journal of Applied Physics, vol. 93, (1), pp. 362-367, 2003.

[52] T. Milakovich, R. Shah, S. Hadi, M. Bulsara, A. Nayfeh and E. Fitzgerald, "Growth and characterization of GaAsP top cells for high efficiency III-V/si tandem PV," in 2015 IEEE 42nd Photovoltaic Specialist Conference, PVSC 2015, 2015, .

[53] T. J. Grassman, D. J. Chmielewski, S. D. Carnevale, Carlin J. A., Ringel S. A., "GaAs0.75P0.25/Si Dual-Junction Solar Cells Grown by MBE and MOCVD,"IEEE Journal of Photovoltaics, vol. 6, (1), pp. 326-331, 2016.

[54] S. Fan et. al., "20%-efficient epitaxial GaAsP/Si tandem solar cells,"Solar Energy Materials and Solar Cells, vol. 202, pp. 110144, 2019.

[55] T. J. Grassman, et al., "Toward >25% efficient monolithic epitaxial GaAsP/si tandem solar cells," in IEEE 46th Photovoltaic Specialists Conference (PVSC), Chicago, IL, USA, 2019, .

[56] C. Algora and I. Rey-Stolle. Handbook on concentrator photovoltaic technology. Wiley. USA. 2016.

[57] M. Meusel, C. Baur, G. Letay, A. W. Bett, W. Warta, E. Fernandez, "Spectral response measurements of monolithic GaInP/Ga(In)As/Ge triple-junction solar cells: Measurement artifacts and their explanation,"Progress in Photovoltaics, vol. 11, pp. 499-514, 2003.

[58] E. Barrigón, P. Espinet-González, Y. Contreras, I. Rey-Stolle, "Implications of low breakdown voltage of component subcells on external quantum efficiency measurements of multijunction solar cells,"Progress in Photovoltaics, vol. 23, pp. 1597-1607, 2015.

[59] E. Barrigón, P. Espinet-González, Y. Contreras, I. Rey-Stolle, "Why can't I measure the external quantum efficiency of the Ge subcell of my multijunction solar cell?"AIP Conference Proceedings, vol. 1679, (050002), 2015.

[60] C. M. Ruiz et. al., "Capacitance measurements for subcell characterization in multijunction solar cells," in 35th IEEE Photovoltaic Specialists Conference, 2010, pp. 00708-000711.

[61] M. Rutzinger, M. Salzberger, A. Gerhard, H. Nesswetter, P. Lugli, C. G. Zimmermann, "Measurement of subcell depletion layer capacitances in multijunction solar cells,"Applied Physics Letters, vol. 111, (183507), 2017.

[62] R. Hoheisel, M. Schachtner, E. Stämmler, A. W. Bett, "Determination of the subcell photovoltage in multijunction solar cells via voltage dependent capacitance analysis,"Applied Physics Letters, vol. 98, (251106), 2011.

[63] L. Barrutia, E. Barrigón, I. García, I. Rey-Stolle, C. Algora, "Effect of Ge autodoping during III-V MOVPE growth on Ge substrates", Journal of Crystal Growth, vol. 475, pp. 378-383, 2017.

[64] W. Li, S. Laaksonen, J. Haapamaa, M. Pessa, "Growth of device-quality GaAs layer directly on (001) Ge substrates by both solid-source and gas-source MBE,"Journal of Crystal Growth, vol. 227-228, pp. 104-107, 2001.